frontiers | Frontiers in Materials

ORIGINAL RESEARCH
published: 05 July 2022
doi: 10.3389/fmats.2022.930633

Effects of Different Fatty Acids as Surfactants on the Rheological Properties of Kerosene-Based Magnetic Fluids

Guobao Zang[1], *Zhili Zhang*[1]*, *Wenjuan Yu*[1], *Deyi Wang*[1] *and Decai Li*[1,2]

[1]Country School of Mechanical Electronic and Control Engineering, Beijing Jiaotong University, Beijing, China, [2]State Key Laboratory of Tribology, Tsinghua University, Beijing, China

Three types of surfactants (oleic acid, linoleic acid, and a mixture of oleic acid and linoleic acid) were coated on ferromagnetic particles, which were dispersed in kerosene to prepare magnetic fluids, to study the effect of different fatty acids as surfactants on the rheological properties of magnetic fluids. The particles were analyzed by XRD, TEM, FT-IR, and VSM. Furthermore, a rheometer was used to examine the rheological properties of kerosene-based magnetic fluids dispersed with various surfactants. The yield stress at different magnetic fields was calculated by fitting the Herschel–Bulkley model. The fitted curve and the observed values of mixed fatty acids are identical. The graphs of viscosity increase with the shear rate for each magnetic fluid were measured at constant magnetic field strengths. At constant shear rates, the curves of viscosity increase with magnetic field intensity were measured. In the absence of a magnetic field, the relative change in viscosity from 40°C to 0°C was observed. The rheological measurements of the mixed fatty acid-dispersed ferrofluid with a rising magnetic field at a constant shear rate are smoother than the single-fatty-acid-dispersed ferrofluid, indicating that it is more stable. As the temperature is dropped, the viscosity–temperature curve evidence that mixed fatty acids as surfactants can lower the proportion of magnetic fluid viscosity rise.

Keywords: magnetic fluids, magnetite, surfactants, kerosene-based, rheological properties

OPEN ACCESS

Edited by:
Yang Yu,
Western Sydney University, Australia

Reviewed by:
U. Ubaidillah,
Sebelas Maret University, Indonesia
Qing Ouyang,
Jiaxing University, China

***Correspondence:**
Zhili Zhang
zlzhang@bjtu.edu.cn

Specialty section:
This article was submitted to Smart Materials, a section of the journal Frontiers in Materials

Received: *28 April 2022*
Accepted: *30 May 2022*
Published: *05 July 2022*

Citation:
Zang G, Zhang Z, Yu W, Wang D and Li D (2022) Effects of Different Fatty Acids as Surfactants on the Rheological Properties of Kerosene-Based Magnetic Fluids. Front. Mater. 9:930633. doi: 10.3389/fmats.2022.930633

1 INTRODUCTION

Magnetic fluids, also known as ferrofluids, are nanocolloids made up of nanometer-sized ferromagnetic particles dispersing in a carrier liquid (typically comprises three parts: base carrier liquid, surfactant, and ferromagnetic particles) (Wang et al., 2018; Dubreuil and Bobowski, 2019). Since the particles are easier to agglomerate, ferromagnetic particles are typically coated with surfactants to prevent agglomeration (Asahi et al., 2011). Magnetic fluids can exhibit both the fluidity of liquids and magnetic properties under an external magnetic field. Hence, magnetic fluids have always received extensive attention and become a research hotspot and have a wide variety of applications because of their fluidity and magnetism (Batter et al., 2013; Cui et al., 2015), including sealing (Li et al., 2017; Marcin, 2018; Szczech, 2020), lubrication (Shahrivar and de Vicente, 2014), sensors (Yao et al., 2015; Yu et al., 2018; Yu et al., 2019), biomedicine (Hensley et al., 2017; Metelkina et al., 2017), and so on. In particular, magnetic fluid sealing is one of the advanced applications of magnetic fluids. Compared with other seals, it has zero leakage, a long life, high rotational speed capability, low viscosity friction, and great reliability. Therefore, it offers significant engineering

application value in aerospace, military equipment, mechanical engineering, and other industries, and broad development potential (Wang and Decai, 2015; Yang et al., 2019).

Magnetic fluid sealing is very suitable for high-end sealing equipment in aerospace and military fields such as missile launchers, tank panoramic mirrors, radar waveguide components, etc. However, in these sealing applications, the start-up resistance torque of the sealing structure is usually strictly required and should be kept within a stable range in any case. Also, magnetic fluid rheological properties are the key factors affecting magnetic fluid sealing (Cheng et al., 2021). It has a significant impact on the starting torque and rotating torque of magnetic fluid rotary seals, and the failure of pressure resistance. In particular, magnetic fluid seals are used in tank panoramic mirrors and radar waveguide components, and the ambient temperature is sometimes very low.

Research on the rheological properties of magnetic liquids mainly focuses on the base carrier liquid and particles (Felicia and Philip, 2012; Paul et al., 2016; Yu et al., 2016; Yang et al., 2020; Cheng et al., 2021). Cheng et al. (2021) studied the effect of rheological properties on seals using magnetic fluids with relatively large viscosity differences between PFPE and diester based. Paul et al. (2016) prepared water-based magnetic liquids with different particle concentrations and studied the non-Newtonian rheological properties of magnetic fluids with different concentrations of viscosity increasing with shear rate, and the non-Newtonian behavior was enhanced by applying a magnetic field. Felicia and Philip (2012) synthesized oil-based ferrofluids and investigated their magnetorheological properties under different magnetic field strengths and volume fractions. They observed a distinct "plateau-like region" in the shear-thinning viscosity curve, under an external magnetic field at extremely small shear rates, and the structure is stable against fragmentation because of a particular alignment of the chains concerning the field direction. Yu et al. (2016) dispersed $Fe_{78}Si_9B_{13}$ amorphous particles into silicone oil to study their rheological properties, confirming that amorphous particles have an improved magnetorheological response compared with magnetic fluids with Fe_3O_4 nanoparticles under an applied magnetic field. Yang et al. (2020) synthesized an Fe_3O_4 hydrocarbon oil-based ferrofluid and its magnetorheological behavior was investigated. A clear hysteresis effect was observed from the viscosity-shear rate flow curve.

Magnetic nanoparticles are uniformly disseminated in the carrier liquid with the assistance of surfactants, which play a crucial role in the magnetic fluid composition (Asahi et al., 2011). Lebedev (2010) prepared mixed fatty acid-modified particles dispersed in isopropanol. Compared with a single oleic acid-modified magnetic liquid, the solidification temperature was reduced to −100°C, which greatly expanded the working range of the magnetic fluid. It is proven that the mixed fatty acid has an important effect on the viscosity of the magnetic fluid at low temperatures. However, surfactant effects on magnetorheological properties have received very little attention. The choice of a surfactant is closely related to the properties of the base carrier fluid, fatty acids are commonly used to stabilize hydrocarbons (Lebedev, 2010), and kerosene is a mixture of hydrocarbons and is commonly used to synthesize magnetic fluids. An oleic acid-stabilized kerosene-based magnetic fluid is the most stable application (Lebedev and Lysenko, 2010). Because of the volatility of kerosene, kerosene-based magnetic fluid seals are usually not used in high-temperature environments, and more choices are used in low-temperature environments. Hao et al. (2015) investigated the viscosity-temperature curves of magnetic fluids with various carrier fluids and demonstrated that the rise in the rotational resistance torque of the magnetic fluid seal was caused by the magnetic fluid's viscosity increasing as the temperature decreased. To make the kerosene-based magnetic fluid used in a lower environment, the surfactant should be chosen with a lower melting point to further minimize the rotating resistance torque of the ferrofluid at low temperatures. The optimum choice is linoleic acid, which has the same chain length as oleic acid and two double bonds. Furthermore, mixing two fatty acids to combine the advantages of two fatty acids is a new approach for better application.

Thence, to investigate the properties of magnetic particles and magnetic fluids, single oleic acid and linoleic acid, and two types of fatty acids combined with modified magnetic fluids, were prepared. Abbreviations for the different surfactants and the meaning of the letters in the figures are shown in **Table 1**. This article aims to further verify and explain the influence of different surfactants on the magnetic fluid by comparing three magnetic fluids with different surfactants modified.

2 MATERIALS AND METHODS

2.1 Materials

Ferric chloride hexahydrate ($FeCl_3{\cdot}6H_2O$), ferrous chloride tetrahydrate ($FeCl_2{\cdot}4H_2O$), and ethanol were procured from Sinopharm Chemical Reagent Beijing Co., Ltd. Ammonium hydroxide ($NH_3{\cdot}H_2O$, 25%), oleic acid ($C_{18}H_{34}O_2$, melting point, 14°C), linoleic acid (C_{18} $H_{32}O_2$, melting point, −5°C), kerosene, and tris(n-nonylphenyl) phosphite were purchased from Beijing Chemical Reagents Company. All compounds are analytical grade and are used without being purified further.

2.2 Experiments

Chemical co-precipitation is the most widely used method to prepare Fe_3O_4 nanoparticles, and the reaction is $Fe^{2+} + 2Fe^{3+} + 8OH^- \rightarrow Fe_3O_4 \downarrow + 8H_2O$. Considering that ferrous irons would be oxidized to ferric irons in the air, the molar ratio of Fe^{2+}: Fe^{3+} was 1:1.75. Taking 20.85 g $FeCl_3 \cdot 6H_2O$ and 8.85 g $FeCl_2 \cdot 4H_2O$ dissolved in 300 ml deionized water under mechanical stirring at 60°C–70°C, ammonium hydroxide was added to the mixed solution whose color changed from red-brown to black immediately and reacted for 30 min under mechanical stirring of 300 rad min^{-1}. Afterward, it heats up to 70°C, keep stirring, and OA as a surfactant was added to the mixture solution for 1 h. Then modified Fe_3O_4 NPs could be obtained by centrifugation or magnetic sedimentation through a

TABLE 1 | Labels for different samples and their meanings.

Labeling of different samples	Meanings
OA	Oleic acids
LA	Linoleic acids
MA	Mixed fatty acids of oleic and linoleic acids
MOA	Oleic acid-coated magnetic nanoparticles and their corresponding magnetic fluids
MLA	Linoleic acid-coated magnetic nanoparticles and their corresponding magnetic fluids
MMA	Mixed fatty acid-coated magnetic nanoparticles and their corresponding magnetic fluids

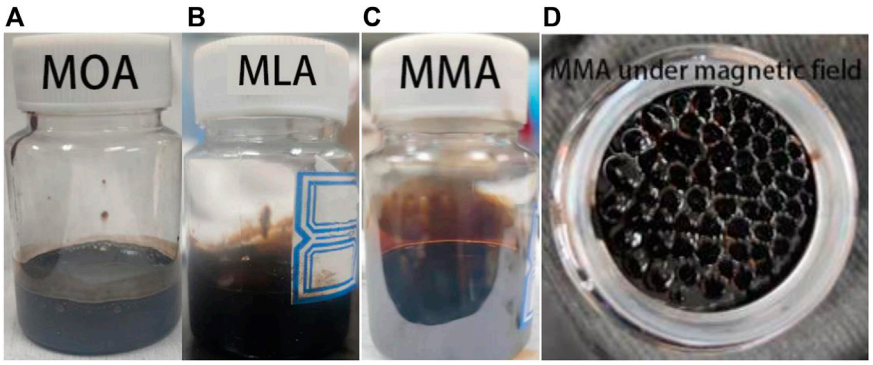

FIGURE 1 | Prepared images of **(A)** MOA, **(B)** MLA, **(C)** MMA, and **(D)** MMA under a magnetic field.

permanent. The modified Fe_3O_4 NPs were washed with ethanol or ultra-pure water several times until the pH was 7 and dried in a vacuum oven for 8 h at 60°C. LA and MA (which could be mixed with ethanol or ultra-pure water, the ratio of oleic and linoleic was 1:1) were used as surfactants to modify the magnetic nanoparticles by the same preparation process. Finally, the quantitative Fe_3O_4 NPs were dispersed in kerosene by ultrasonic for 2 h to obtain a stable magnetic fluid.

For kerosene-based magnetic fluids containing LA, antioxidants are finally added to prevent the oxidation of linoleic acid. The prepared MLA is added with a little tris(*n*-nonylphenyl) phosphite.

The magnetic fluids dispersed with different surfactants are shown in **Figures 1A–C**. **Figure 1D** shows the response of MMA under a magnetic field.

2.3 Characterization of Nanoparticles

The synthesized nanoparticles were characterized by X-ray diffraction (XRD), transmission electron microscopy (TEM), infrared spectroscopy (IR), and vibrating sample magnetometry (VSM) to identify the shape, size, surfactant coating type, and magnetic properties of the samples.

XRD using a D8 Advance Bruker AXS diffractometer with a scan speed of 0.1° per second in the range of 20°–80° was used to determine the identity, phase, and crystallite size of the produced powder sample.

The morphology and nanoparticle size was characterized with a JEM-F200 transmission electron microscope (TEM). The nanoparticles were diluted sufficiently with ethanol and a single drop of the liquid suspension was deposited on a duplex copper mesh. The sample is dried by allowing the ethanol to evaporate through the double copper mesh for a length of time.

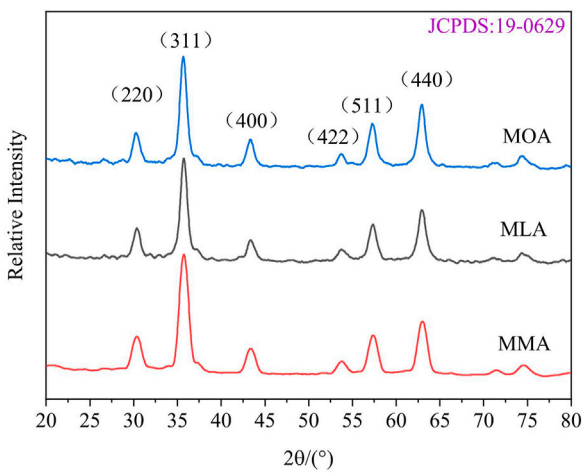

FIGURE 2 | XRD images of Fe_3O_4 particles in three magnetic fluids.

The Fe_3O_4@*OA*, Fe_3O_4@*MFA*, and Fe_3O_4@*LA* nanoparticles were first defined for the functional groups by using an FT-IR spectrometer (NETZSCH, X70). The scanning range of the infrared spectrum is 4,000 cm^{-1}–600 cm^{-1}.

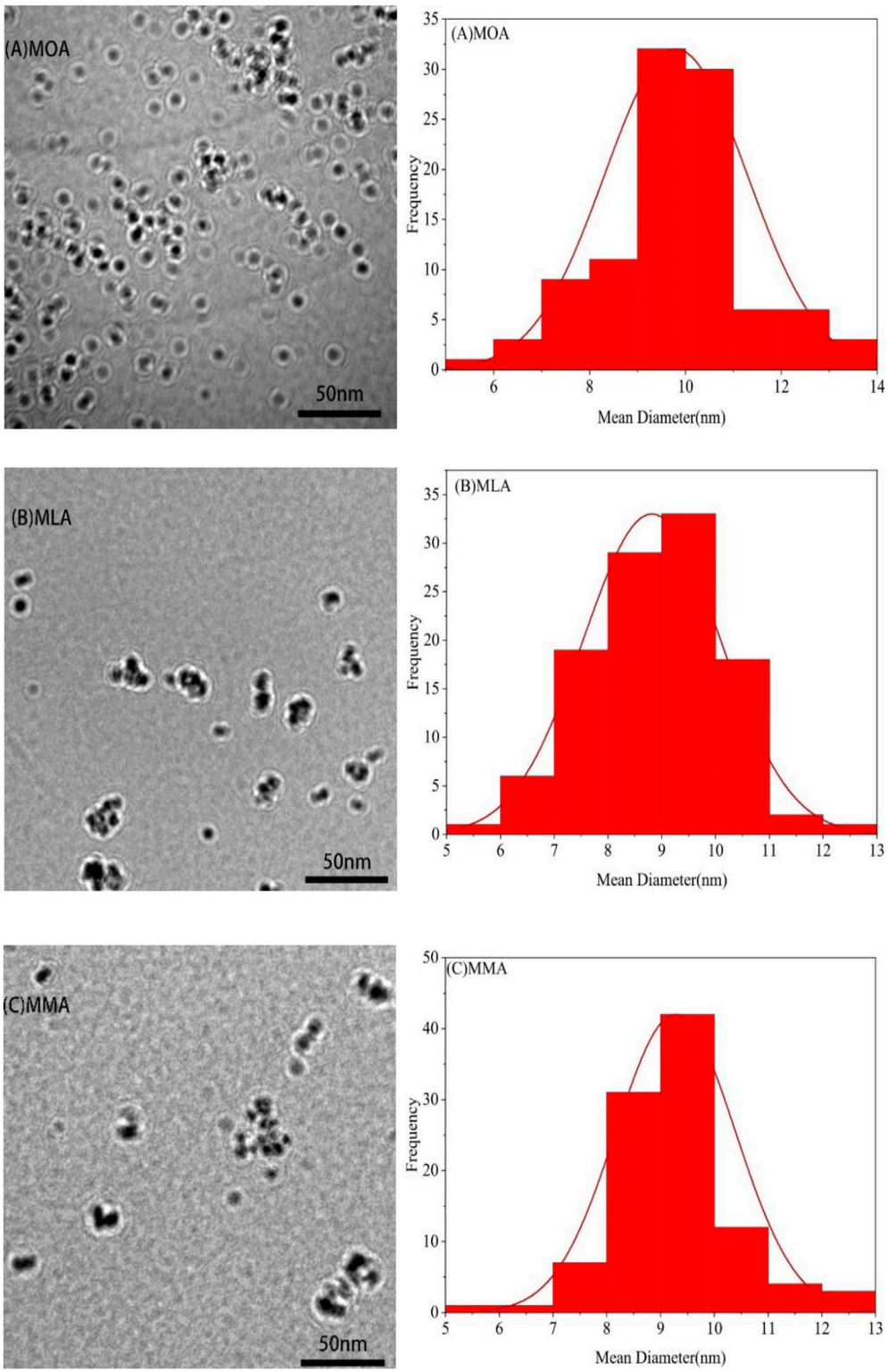

FIGURE 3 | TEM images of particles in three magnetic fluids (left) and the corresponding particle size distribution histograms (right).

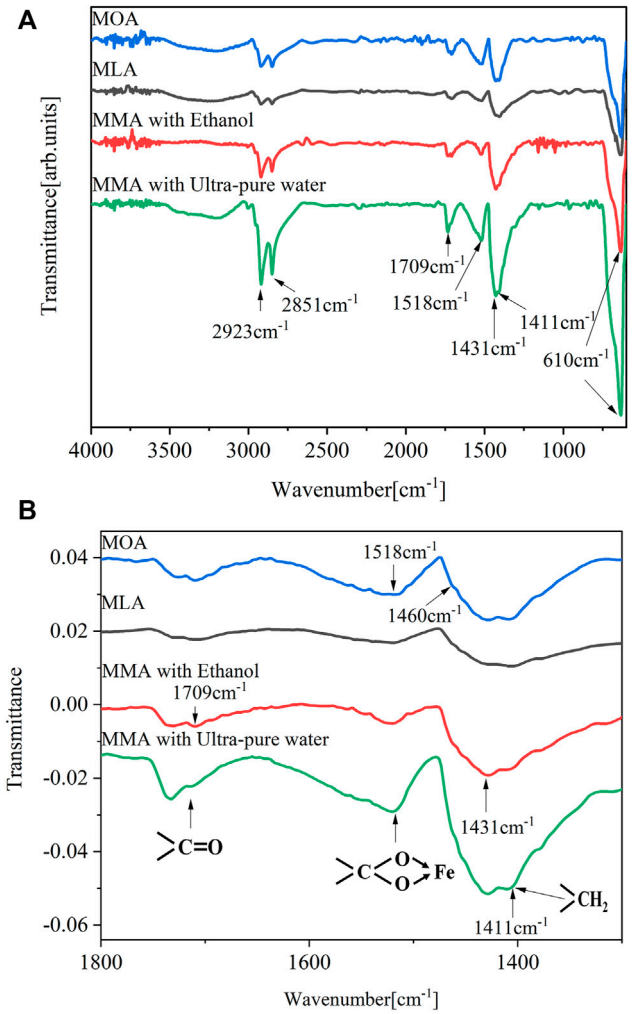

FIGURE 4 | (A) Infrared spectra images of particles in three magnetic fluids, **(B)** 1,300–1800 cm^{-1} zoomed spectra in the carboxylate region.

Magnetic measurements were performed at room temperature on a vibrating sample magnetometer (VSM, LakeShore, model 7307) in a ± 8 kOe external magnetic field.

The rheological properties of the samples were investigated using an MCR302 rheometer, M/s Anton Paar GmbH. A special plate–plate spindle, CP20-MRD, was used for all the measurements in a magnetic field. A coaxial magnetic field in the perpendicular direction to the sample was applied during the rheological measurement. A thermostatic bath (±0.1°C) was used to maintain a constant temperature of the samples during rheology tests. The gap between the plates was 0.084 mm unless otherwise mentioned.

3 RESULTS AND DISCUSSION

3.1 X-Ray Diffraction Analysis

The XRD pattern of the prepared nanoparticles with coating surfactants is shown in **Figure 2**. The crystal structures of Fe_3O_4 nanoparticles using OA, LA, and MA as surfactants are confirmed by an XRD analysis as shown in **Figure 2**. The peak at 30.3°, 35.6°, 43.2°, 53.8°, 57.2°, and 62.8° can be indexed to (2 2 0), (3 1 1), (4 0 0), (4 2 2), (5 1 1), and (4 4 0) lattice planes, respectively, characteristic of Fe_3O_4, which is confirmed by JCPDS card no: 19-0629. The pattern of the three nanoparticles is almost identical, which implies that the modification will not affect the Fe_3O_4 crystal phase of the inverse spinel structure. The average crystallite size of the samples is calculated from the width of the major peak corresponding to the (311) plane using the Scherrer equation.

$$D = \frac{0.9\lambda}{\beta \cos \theta}, \tag{1}$$

where D is the average crystallite size, λ is the wavelength of X-rays, β is full width at half maximum of the peak after correcting the instrumental contribution to the peak broadening, and θ is the angle of diffraction. The calculated particle sizes of the OA, LA, and MA-modified particles are 9.3, 8.7, and 9.5 nm, respectively.

3.2 Transmission Electron Microscope Analysis

The TEM images of the magnetite nanoparticles at high magnifications (left) and the corresponding particle size distribution histograms (right) are shown in **Figures 3A–C**, respectively. The magnetite nanoparticles are observed to be nearly spherical. The particle size distribution histogram, shown in **Figure 3** (right), has been constructed from the image analysis of a series of TEM images. The average particle size was calculated from the micrographs as 9.8, 8.8, and 9.3 nm with a standard deviation of 1.49, 1.28, and 1.1 for OA, LA, and MA-modified particles, respectively. The particle size distribution observed from TEM fairly matches that observed from XRD.

3.3 Infrared Spectroscopy Analysis

Figure 4A compares the infrared spectra of fatty acid-coated powder samples. The Fe-O stretching vibration of Fe_3O_4 corresponds to 610 cm^{-1} (Lenin and Joy, 2017). The symmetric and asymmetric stretching vibrations of methylene (-CH_2-) groups in the fatty acid molecule are represented by the two bands at 2,851 cm^{-1} and 2,923 cm^{-1}, respectively, in all spectra. The bands at 1,411 cm^{-1} and 1,431 cm^{-1} in the spectra of the free acid and the coated particles correspond to -CH_2- deformation. The intensities of OA and MA-coated part bands are higher than those of single LA-coated particles because of increasing unsaturation (-CH=CH-) in the carbon chain. The carbonyl (-C=O) stretching vibration of free fatty acids is represented by the weak band at 1,709 cm^{-1} in all samples. These free fatty acid molecules are most likely caused by the secondary layer present on the surface of the nanoparticles, which is attached to the chemically bound primary layer of fatty acid molecules *via* a weak hydrophobic interaction.

As shown in **Figure 4B**, the bands observed in the range of 1800 cm^{-1}–1,300 cm^{-1} correspond to metal carboxylates, which are

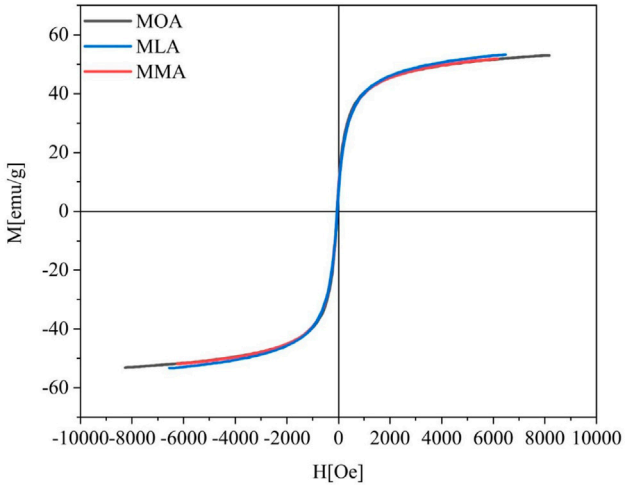

FIGURE 5 | Magnetization curve of particles in three magnetic fluids.

in the range of 1,650 cm^{-1}–1,510 cm^{-1} for the asymmetric carboxyl vibration and 1,431 cm^{-1} for the symmetric carboxyl vibration. The position and separation of carboxyl bands, Δ, deduced the carboxylate coordination mode. More than 200 cm^{-1} indicates monodentate, between 200 and 140 cm^{-1} indicates a bridged bidentate ligand, and less than 110 cm^{-1} indicates a chelating bidentate. For all samples, the difference between the two characteristic bands at 1,518 cm^{-1} and 1,431 cm^{-1} is 87 cm^{-1}, revealing bidentate coordination. The 1,431 cm^{-1} band's location is unknown since it may occur from the overlapping of the carboxylate (COO-) stretching and methylene (-CH_2-) scissoring bands. The shoulder on the peak at 1,431 cm^{-1} is around 1,411 cm^{-1}, making Δ = 104 while still meeting the bidentate coordination (Bronstein et al., 2007; Lenin and Joy, 2016). The intensity of the bands is affected by the washing method used. Moreover, different mixing methods have a huge impact on the intensity of the bands for MA-coated nanoparticles. Peak intensities are much higher when ultra-pure water-mixed fatty acids are used as surfactants than when other surfactants are used. When compared with the fatty acids, the strength of the carbon-based tape at 1709 cm^{-1} in **Figure 4B** decreased significantly after coating (Bronstein et al., 2007). All coated samples had only a weak band at 1709 cm^{-1}, indicating that only a small amount of free acid groups were present. However, the bands of ultra-pure water mixed-fatty acids have a stronger intensity than those of other surfactants, indicating that more free acid is excited.

The carboxylic acid group is bonded to the surface of the nanoparticles, according to the IR analyses. The variation in the conformation of the surfactant molecules, which directly impacts the number of molecules bound to the surface of the nanoparticles, might explain the decrease in the strength of the symmetric and asymmetric stretching of the carboxylate group.

3.4 Vibration Sample Magnetometer Analysis

Magnetic properties of different surfactant-modified nanoparticles are measured at 300 K, at ±8 kOe, as shown in **Figure 5** Magnetization is the most distinctive physical property for ferrofluids. The saturation magnetization of OA, LA, and MA-dispersed magnetic fluid is 53.4, 50.2, and 52.8 emu/g, respectively, and the observed tiny changes in magnetization are consistent with the observed particle size from the TEM histogram (**Figure 3**). The nanoparticles exhibit super-paramagnetism similar to bulk magnetic material, but they have no residual magnetism or remanence when the magnetic field is removed, and particles with different surfactant-modified nanoparticles exhibit excellent super-paramagnetism.

3.5 Rheological Property Analysis

3.5.1 Effect of Shear Rate on Shear Stress

To compare the properties of several magnetic fluids more clearly, **Table 2** gives the density of the magnetic fluid, and the particle size and saturation magnetization of the particles measured by TEM and VSM.

The shear rate of different surfactant-coated magnetic fluids' dependence on the effect of shear stress is shown in **Figures 6A–C**. At room temperature (20°C), rheological studies for various coated magnetic fluids were carried out by altering the shear rate in the range of 0–500 s^{-1}. The samples have been subjected to pre-shearing for about 200 s at a shear rate of 500 s^{-1} without recording any data.

In the absence of a magnetic field, the shear stress increases linearly with the shear rate. In the presence of a magnetic field, the shear stress increases nonlinearly with the increase of the shear rate at a constant magnetic field strength, and there is yield stress. Each solidus line in **Figures 6A–C** shows the fitted values of the flow curves by the power-law relation as predicted by the Herschel–Bulkley model given by

$$\tau = \tau_{H-B} + k \cdot \dot{\gamma}^n,$$

where τ_{H-B} is the yield stress under the magnetic field strength H and k, $\dot{\gamma}$, and n are the consistency parameter, shear rate, and power-law index, respectively. As shown in **Figures 6A–C**, the value of shear stress increases with increasing shear rate. At a constant magnetic field of 200 mT, the fitted curve of the single fatty acid-modified magnetic fluids deviates slightly from the experimental value at a high shear rate. However, the simulation value of the MMA is most consistent with the experimental value. The yield stress is related to the actuation torque in the magnetic fluid seal and a higher viscosity fluid has a higher starting torque of seals (Cheng et al., 2021). The magnetic fluids can flow freely only when the applied force is greater than the yield stress.

The numerical values of and k,$\dot{\gamma}$, and n for different applied constant magnetic fields for each of the three magnetic fluids are shown in **Table 3**. It can be seen that all the magnetic fluids have n < 1 under different magnetic fields, indicating that the fluid is shear thinning, and different surfactants dispersed in the magnetic fluids will not affect the shear-thinning phenomenon.

Under the action of the magnetic field, the force of the interparticle interaction hindering the movement of the fluid leads to the appearance of yield stress. **Figure 6D** shows the fitted yield stress of magnetic fluids with different magnetic fluids under different constant magnetic fields. The figure

TABLE 2 | Parameters of three magnetic fluids at 20°.

Symbol	Meaning	MOA	MLA	MMA
ρ	Magnetic fluid density	1.14 g/cm^3	1.25 g/cm^3	1.17 g/cm^3
d	Particle diameter from TEM	9.8 nm	8.8 nm	9.3 nm
M_S	Particle saturation magnetization	53.4 emu/g	50.2 emu/g	52.8 emu/g

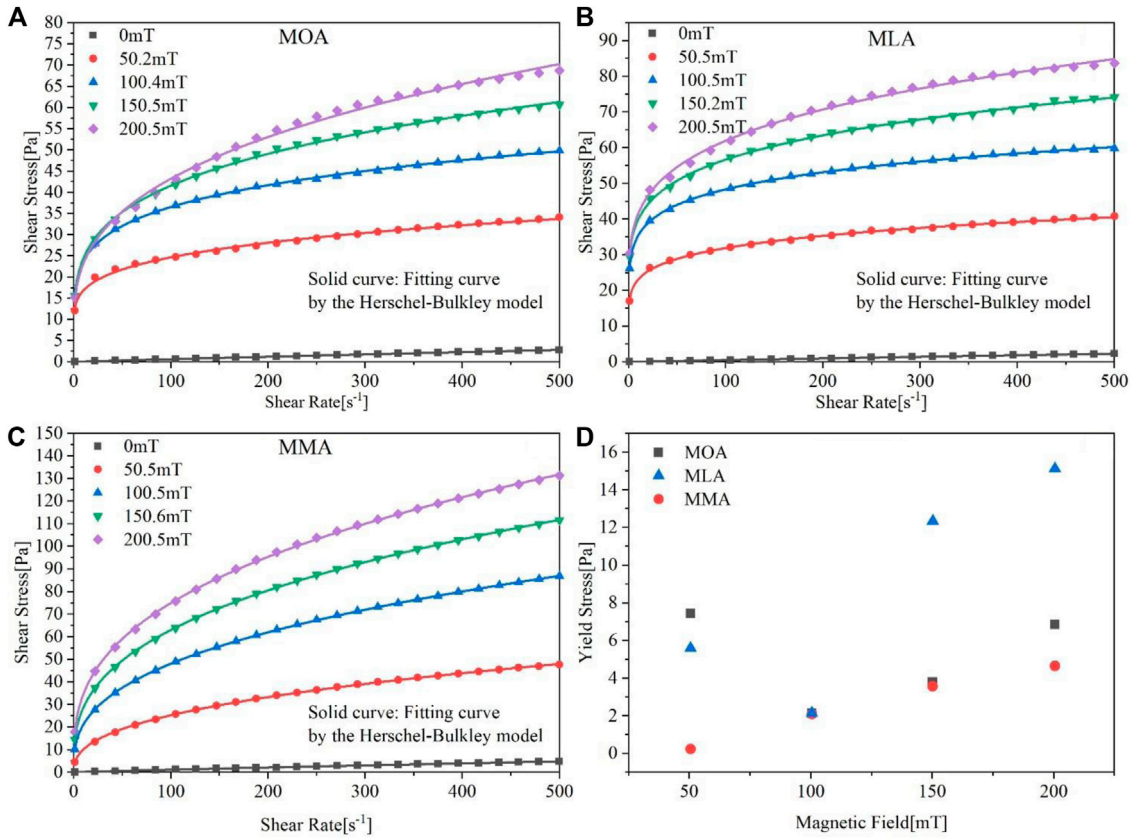

FIGURE 6 | Stress-strain images of **(A)** MOA, **(B)** MLA, and **(C)** MMA. **(D)** Fitted yield stress values of three magnetic fluids by the Herschel–Bulkley model under a constant magnetic field.

TABLE 3 | Rheometric parameters estimated by fitting the Herschel–Bulkley model to the shear stress variation with the shear rate.

Magnetic fluid type	Coefficient value	Applied magnetic field, H			
		50.5 mT	100.5 mT	150.2 mT	200.5 mT
MOA	Yield stress, τ_{H-B}	7.42693	2.13692	3.79829	6.84633
	Consistency parameter, *k*	5.15828	13.65195	11.36512	7.41169
	Power law index, *n*	0.26212	0.20077	0.26093	0.34545
MLA	Yield stress, τ_{H-B}	5.58165	2.14793	12.33298	15.11992
	Consistency parameter, *k*	11.67134	24.03183	17.20449	15.00951
	Power law index, *n*	0.17655	0.14195	0.20561	0.24716
MFA	Yield stress, τ_{H-B}	0.23542	2.10149	3.56683	4.64928
	Consistency parameter, *k*	3.9549	7.99188	10.72927	12.88907
	Power law index, *n*	0.40082	0.38015	0.37184	0.36834

shows that the yield stress of different magnetic fluids increases with increasing constant magnetic field strength, and the dynamic yield stress at a higher magnetic fields indicates that the formation of a large number of chain structures hinders the flow (Felicia and Philip, 2012). Yield stress of the MMA increases with the increase in the magnetic

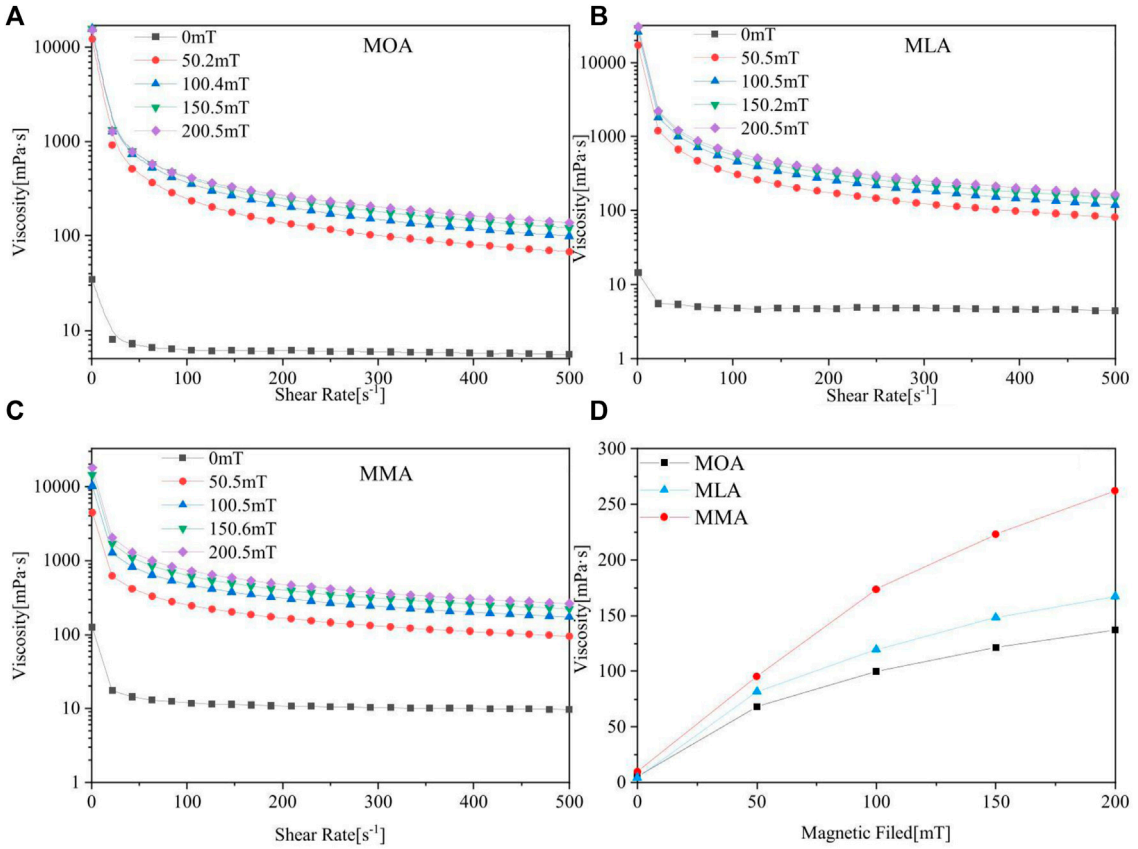

FIGURE 7 | Viscosity-strain images of **(A)** MOA, **(B)** MLA, and **(C)** MMA. **(D)** Maximum shear rate limiting viscosity-constant magnetic field comparison images of three magnetic fluids.

field. While the yield stress at 50 mT for MOA shows an unusual increase and MLA shows a decrease at 100 mT, depending on the choice of data points in the curve, the higher shear rate value affects to some extent. The determination of the fitting equation has an impact on the yield stress obtained from the fitting and an error occurs.

However, it will not affect the overall judgment. The reaction of MLA to the magnetic field is still better, wherefore it has larger yield stress, while the yield stress values of MOA and MMA vary in a similar range, and the performance of MMA is more stable.

3.5.2 Effect of Shear Rate on Viscosity

The dependence of viscosity on the shear rate has been studied under the shear rate-controlled measurements for high values of shear rate (0–500 s^{-1}), MOA, MLA, and MMA as shown in **Figures 7A–C**, respectively. The flow curves of magnetic nanofluids under the influence of a magnetic field exhibit shear-thinning non-Newtonian behavior. The non-linearity observed in the flow curves for the different coats of the magnetic nanofluids depicts the pseudo-plastic behavior of the system.

In the absence of a magnetic field, the viscosity (the viscosity value of each magnetic fluid is about 8 mpa s) of ferrofluids is slightly greater than that of kerosene (20°C, 2.5 mpa s). When a magnetic field is applied, the nanoparticles form chain-like structures, which induce fluid motion resistance and as a result, a rise in viscosity (Zubarev et al., 2002). When the magnetic field strength is 50 mT, many chain-like structures are formed, which increase the fluid resistance and the viscosity performance. With the increase in the magnitude of the applied field, the lengths of the chains also increase. It can be seen from **Figures 7A–C** that the viscosity value of magnetic fluids is closer at higher magnetic field strengths of 100, 150, and 200 mT. Each magnetic fluid has the same trend of change. With the increase in shear rate, the viscosity decreases rapidly, and up to a certain shear rate (about 200 s^{-1}) above which the rate of decrease slows down.

It is pertinent to mention that the increase in viscosity takes place only in the low shear rate region while shear thinning occurs for the remaining applied shear rates. Similar shear-thinning behavior with enhanced viscosity under the application of a magnetic field has been earlier reported (Hosseini et al., 2010; Nowak et al., 2014; Shahnazian et al., 2016). The applied magnetic field causes a strong interaction between the magnetic nanoparticles and leads to the formation of magnetic structures. But with the increase in shearing rate, structures in the form of agglomerates tend to break down and the nanoparticles arrange themselves along

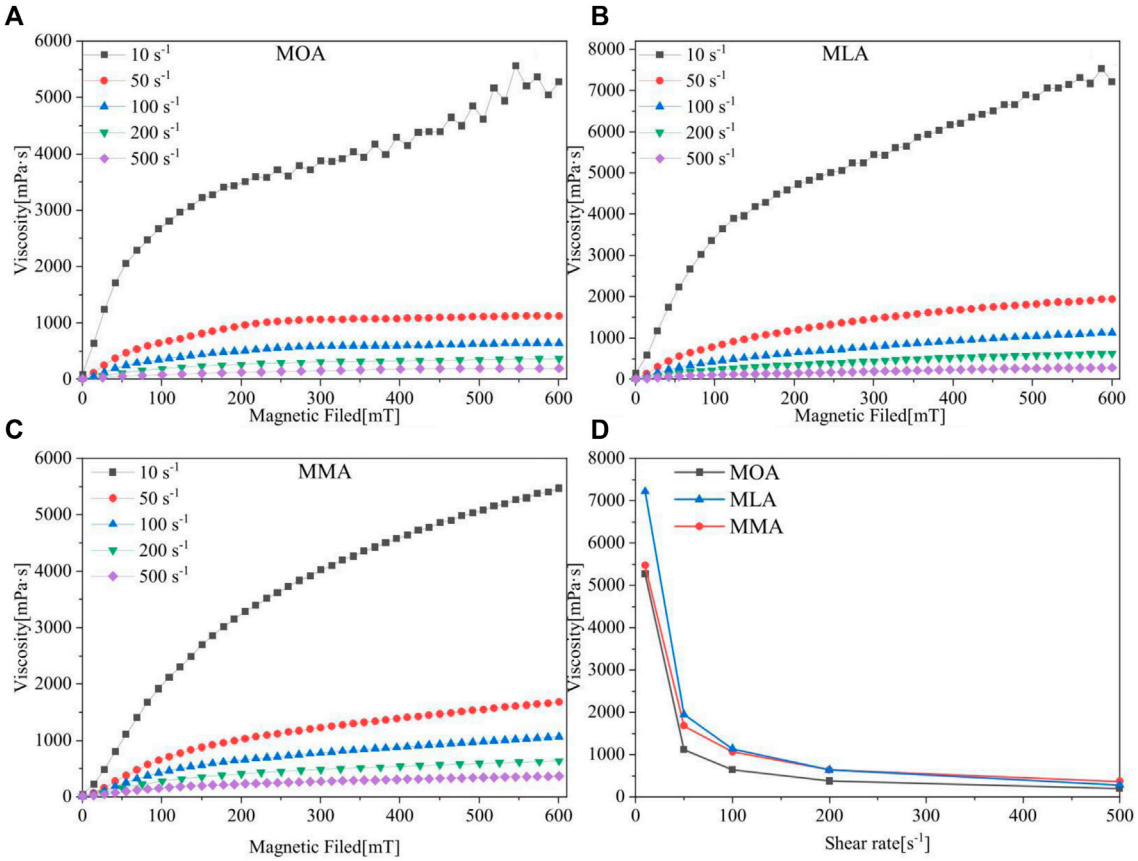

FIGURE 8 | Viscosity-magnetic field images of **(A)** MOA, **(B)** MLA, and **(C)** MMA. **(D)** Maximum magnetic field limit viscosity-constant shear rate comparison images of three magnetic fluids.

the shearing direction. This leads to a decrease in the fluid viscosity at high shear rates (Felicia and Philip, 2012).

The viscosity of the nanofluids at the highest shear rates is called the high shear limiting viscosity, as shown in **Figure 7D**. Thus, it may be noted that the structures that are formed by the application of a magnetic field, although broken down by the application of a high shear rate but are not completely destroyed, has a strong effect on the limiting viscosity of the magnetic fluids. **Figure 7D** shows that when the shear rate increases, the viscosity of the MMA becomes greater than that of the single acid-dispersed magnetic fluids, and a greater slope of viscosity increases the curve. The structure created by the particles of the MMA was influenced more by the action of shear and shows a gradual increase in viscosity. The shear rate has a minor influence, and the performance is more stable.

3.5.3 Effect of Magnetic Field on Viscosity

The magneto-viscous effect was investigated by increasing the magnetic field from 0– 600 mT at different shear rates, as shown in **Figures 8A–C**, respectively. Before each start, pre-shearing was performed for 90 s without a magnetic field and this part of the data was not recorded. During the experiment, the shear rate was kept constant. When a magnetic field is applied, magnetic nanoparticles are polarized and arrange their orientation along the direction of the magnetic field. The nanoparticles form a chain-like structure, causing motion resistance of the fluid and a continuous rise in viscosity.

As the strength of the magnetic field increases, the length of the chains also increases, the shear rate remains constant, and with further increases in the field, multiple chains attract each other, forming a columnar structure that further increases the viscosity of the fluid. After most of the nanoparticles present in the nanofluid dispersion participated in the formation of the column structure, a further increase in the applied field resulted in no further increase in viscosity and reached a saturation value. It is worth mentioning here that a higher dispersion concentration means a higher number and density of nanoparticles. Under an applied magnetic field, the chain-like structures that eventually formed the pillars contained more nanoparticles than the chain-like structures (Felicia and Philip, 2012).

The shear rate has a significant effect on the viscosity of the magnetic fluids with the magnetic field. The viscosity change value under the magnetic field from 0– 200 mT is expanded. Under the influence of the magnetic field, the particles

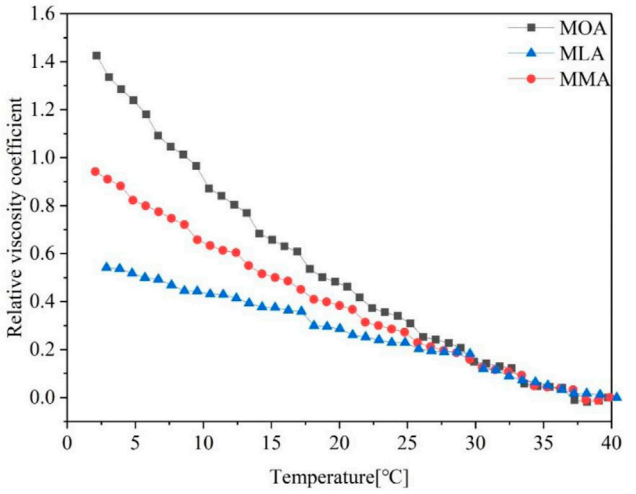

FIGURE 9 | Relative viscosity coefficient-temperature images of three magnetic fluids.

continuously form chain-like formations and are sheared. The shear rate is 10 s^{-1}, and the magnetic field strength of various modified magnetic fluids increased dramatically with the rising magnetic field strength at a low field strength, practically linearly increasing. The shear force was insufficient at the moment to disintegrate the particles' structure and increase the shear rate. The shear rate is 50 s^{-1}, and the massive shear force decomposes the particle-forming structure, resulting in a significant decrease in the degree of reactivity of different magnetic fluids to the magnetic field. Under a magnetic field, the shear force is substantially larger than the yield stress. The viscosity change is further minimized as the shear rate is increased.

The viscosity of all magnetic fluids increases as the magnetic field intensity increases, and the viscosity value progressively tends to be saturated at the highest magnetic field strength, as shown in **Figures 8A–C**. **Figure 8D** shows the change in the viscosity value with an increasing constant shear rate at a magnetic field strength of 600 mT.

When the magnetic field is 600 mT and the shear rate is 10 s^{-1}, the viscosity value of the MLA is 7,300 mpa s higher than that of the MOA and MMA 5,400 mpa s, showing a stronger magneto-viscosity effect. With the increasing shear rate, the viscosity value of the MMA is higher than that of the single fatty acid-modified magnetic fluids at 600 mT, which is consistent with the effect of viscosity on the shear rate. The shear rate is 10 s^{-1}, the single fatty acid-dispersed magnetic fluids both fluctuated at the highest magnetic field strength, and the cause of the oscillations could be the particles' instability as they reorganized. Even with a high magnetic field intensity and a moderate shear rate, the viscosity of the MMA gradually increases, and the performance becomes more stable.

3.5.4 Effect of Temperature on Viscosity

From 40°C to 0°C, the viscosity variations of several magnetic fluids were measured in the absence of a magnetic field. A pre-shear of 100 s^{-1} for 180 s was conducted before that. This portion of the data will not be saved, and it was kept at 100 s^{-1} throughout the experiment. The shear rate remains constant.

Because the viscosity values of different modified magnetic liquids differ at 40°C, the relative viscosity coefficient is used to express the relationship between viscosity and temperature.

$$R = \frac{\eta - \eta_0}{\eta_0}, \tag{2}$$

where R, η, and η_0 are the relative viscosity coefficient, viscosity values at different temperatures, and viscosity values at 40°C, respectively. The relative change in viscosity with temperature is shown in **Figure 9**. When the temperature is reduced to 0°C from 40°C, the viscosity of the MOA increases by 1.5 times. The viscosity of the MLA, on the other hand, increased by 0.6 times. When the temperature lowers to 0°C from 40°C, the viscosity of the MMA doubles, as seen in the figure. On the one hand, different magnetic fluids have different initial viscosity values at 40°C, and on the other hand, this could be due to the surfactant affecting the temperature-induced viscosity shift. Mixed surfactants can ameliorate the viscosity–temperature properties of magnetic fluids to some extent.

Therefore, when the ambient environment of kerosene-based or other hydrocarbon magnetic fluids is at a certain low temperature, it can be considered to use a single fatty acid with a lower melting point to disperse, or a fatty acid with a lower melting point can be mixed with oleic acid. The starting torque of the magnetic fluid seal is related to the amount of viscosity rise at low temperatures. To content the performance, for example, magnetic fluids with good viscosity–temperature performance are required for magnetic liquid sealing in tank panoramic mirrors and radar waveguide components, etc. At this time, surfactant-dispersed magnetic fluids with lower melting points can play an important role. This allows kerosene-based magnetic fluid seals to be used across a wider temperature range.

4 CONCLUSION

The dispersion of several fatty acid-modified particles into kerosene was examined in this work. The following conclusions can be drawn from particle characterization and rheological experiments on magnetic fluids.

1) The particle size will be impacted to some extent when the particles are adjusted by different surfactants, but the crystal phase structure of the particles will not be changed. Bidentate coordination patterns between fatty acids and particles are identified by infrared spectroscopy. MA (mixed fatty acids) have no effect on the coordination mode.

2) The Herschel and Bulkley model was used to fit the stress-strain curve, and the fitted curve for the MMA perfectly matched the experimental value. Under a given magnetic field and a shear rate of 500 s^{-1}, the viscosity of the MMA grows larger than that of single acid-dispersed magnetic fluids, with a greater slope of the viscosity growth curve. This indicates that the mixed fatty acids have more stable rheological properties.
3) When the temperature is changed from 40°C to 0°C, it demonstrates that using a mixed fatty acid as a surfactant can improve the viscosity–temperature performance of magnetic fluids by adjusting the increase ratio of viscosity as the temperature decreases. This work provides a new technique to optimize the viscosity–temperature performance of kerosene-based magnetic fluids when used in low-temperature situations and can lower the increase in the starting torque when magnetic fluids are sealed. Magnetic fluid seals based on kerosene or hydrocarbons can withstand lower ambient temperatures by using surfactants with lower melting points, allowing for a wider application range.

DATA AVAILABILITY STATEMENT

The original contributions presented in the study are included in the article/Supplementary Material; further inquiries can be directed to the corresponding author.

AUTHOR CONTRIBUTIONS

ZZ was in charge of the whole trial; GZ wrote the manuscript and performed laboratory analyses; WY participated in rheological experiments; and DW and DL contributed to the revision of the manuscript.

FUNDING

This work was supported by the National Natural Science Foundation of China major instrument development project (51927810).

REFERENCES

Asahi, T., Koshi, T., Hatsugai, S., Yamada, T., and Takemura, Y. (2011). Magnetic Characterization of Surface-Coated Magnetic Nanoparticles for Biomedical Application. *J. Magnetism Magnetic Mater.* 323, 1398–1403. doi:10.1016/j.jmmm.2010.11.054

Batter, B., Qu, Y., Meng, X., Tian, C., Du, S., Wang, R., et al. (2013). Preparation and Magnetic Performance of the Magnetic Fluid Stabilized by Bi-surfactant. *J. Magnetism Magnetic Mater.* 332, 151–156. doi:10.1016/j.jmmm.2012.12.009

Bronstein, L. M., Huang, X., Retrum, J., Schmucker, A., Pink, M., Stein, B. D., et al. (2007). Influence of Iron Oleate Complex Structure on Iron Oxide Nanoparticle Formation. *Chem. Mat.* 19 (15), 3624–3632. doi:10.1021/cm062948j

Cheng, Y., Li, D., and Li, Z. (2021). Influence of Rheological Properties on the Starting Torque of Magnetic Fluid Seal. *IEEE Trans. Magnetics* 57, 4600308. doi:10.1109/tmag.2019.2934716

Cui, H., Li, D., and Zhang, Z. (2015). Preparation and Characterization of Fe3O4 Magnetic Nanoparticles Modified by Perfluoropolyether Carboxylic Acid Surfactant. *Mater. Lett.* 143, 38–40. doi:10.1016/j.matlet.2014.12.037

Dubreuil, J., and Bobowski, J. S. (2019). Ferromagnetic Resonance in the Complex Permeability of an Fe_3O_4-Based Ferrofluid at Radio and Microwave Frequencies. *J. magnetism magnetic Mater.* 489, 1653871–1653876. doi:10.1016/j.jmmm.2019.165387

Felicia, L. J., and Philip, J. (2012). Probing of Field-Induced Structures and Tunable Rheological Properties of Surfactant Capped Magnetically Polarizable Nanofluids. *Langmuir* 29, 110–120. doi:10.1021/la304118b

Hao, D., Li, D., Chen, J., and Yu, J. (2015). Theoretical Analysis and Experimental Study of the Characteristics of Magnetic Fluid Seal with a Large Diameter at High/low Temperatures. *Int. J. Appl. Electromagn. Mech.*, 58:531–550. doi:10.3233/JAE-180065

Hensley, D., Zhi, W. T., and Dhavalikar, R. (2017). Combining Magnetic Particle Imaging and Magnetic Fluid Hyperthermia in a Theranostic Platform. *Phys. Med. Biol.* 62 (9), 3483–3500. doi:10.1088/1361-6560/aa5601

Hosseini, M., Fazlali, A., Ghasemi, E., and Moghaddam, H. (2010). Rheological Properties of a γ-Fe2O3 Paraffin-Based Ferrofluid. *J. Magnetism Magnetic Mater.* 22 (23), 3792–3796. doi:10.1016/j.jmmm.2010.08.003

Lebedev, A. V. (2010). Low-temperature Magnetic Fluid Stabilized with Mixed Fatty Acids. *Colloid J.* 72 (6), 815–819. doi:10.1134/s1061933x10060128

Lebedev, A. V., and Lysenko, S. N. (2010). Magnetic Fluids Stabilized by Polypropylene Glycol. *J. Magnetism Magnetic Mater.* 323 (10), 1198–1202. doi:10.1016/j.jmmm.2010.11.005

Lenin, R., and Joy, P, A. (2016). Role of Primary and Secondary Surfactant Layers on the Thermal Conductivity of Lauric Acid Coated Magnetite Nanofluids. *J. Phys. Chem. C. Nanomater. interfaces*, 120:11640–11651. doi:10.1021/acs.jpcc.5b12476

Lenin, R., and Joy, P. A. (2017). Studies on the Role of Unsaturation in the Fatty Acid Surfactant Molecule on the Thermal Conductivity of Magnetite Nanofluids. *J. Colloid Interface Sci.* 506, 162–168. doi:10.1016/j.jcis.2017.07.038

Li, Z., Li, D., Chen, Y., Yilong, Y., and Yao, J. (2017). Influence of Viscosity and Magnetoviscous Effect on the Performance of a Magnetic Fluid Seal in a Water Environment. *Tribol. Trans.*, 61:367–375. doi:10.1080/10402004.2017.1324071

Marcin, S. (2018). Experimental Study on the Pressure Distribution Mechanism Among Stages of the Magnetic Fluid Seal. *IEEE Trans. Magn.* 54, 1–7. doi:10.1109/tmag.2018.2816567

Metelkina, O. N., Lodge, R. W., Rudakovskaya, P. G., Gerasimov, V. M., Lucas, C. H., Grebennikov, I. S., et al. (2017). Nanoscale Engineering of Hybrid Magnetite-Carbon Nanofibre Materials for Magnetic Resonance Imaging Contrast Agents. *J. Mat. Chem. C* 5 (8), 2167–2174. doi:10.1039/c6tc04141h

Nowak, J., Wolf, D., and Odenbach, S. (2014). A Rheological and Microscopical Characterization of Biocompatible Ferrofluids. *J. Magnetism Magnetic Mater.* 354 (mar), 98–104. doi:10.1016/j.jmmm.2013.10.050

Paul, G., Kumar Das, P., and Manna, I. (2016). Synthesis, Characterization and Studies on Magneto-Viscous Properties of Magnetite Dispersed Water Based Nanofluids. *J. Magnetism Magnetic Mater.* 404, 29–39. doi:10.1016/j.jmmm.2015.11.085

Shahnazian, H., Graf, D., Borin, D. Y., and Odenbach, S. (2016). Rheology of a Ferrofluid Based on Nanodisc Cobalt Particles. *J. Phys. D-Applied Phys.* 49, 279501. doi:10.1088/0022-3727/42/20/205004

Shahrivar, K., and de Vicente, J. (2014). Ferrofluid Lubrication of Compliant Polymeric Contacts: Effect of Non-homogeneous Magnetic Fields. *Tribol. Lett.* 56 (2), 281–292. doi:10.1007/s11249-014-0408-y

Szczech, M. (2020). Experimental Studies of Magnetic Fluid Seals and Their Influence on Rolling Bearings. *J. Magnetics* 25 (1), 48–55. doi:10.4283/JMAG.2020.25.1.048

Wang, J., Fan, M., Bian, X., Yu, M., Wang, T., Liu, S., et al. (2018). Enhanced Magnetic Heating Efficiency and Thermal Conductivity of Magnetic Nanofluids with FeZrB Amorphous Nanoparticles. *J. magnetism magnetic Mater.* 465, 480–488. doi:10.1016/j.jmmm.2018.06.043

Wang, Z., and Decai, L. (2015). Theoretical Analysis and Experimental Study on Loading Process Among Stages of Magnetic Fluid Seal. *Int. J. Appl. Electromagn. Mech.* 48, 101–110. doi:10.3233/JAE-140126

Yang, C., Liu, Z., Yu, M., and Bian, X. (2020). The Influence of Thixotropy on the Magnetorheological Property of Oil-Based Ferrofluid. *J. Mol. Liq.* 320 (3), 114425. doi:10.1016/j.molliq.2020.114425

Yang, X., Sun, P., Chen, F., Hao, F., Li, D., and Thomas, P. J. (2019). *Numerical and Experimental Studies of a Novel Converging Stepped Ferrofluid Seal*. New Jersy(US): IEEE Transactions on Magnetics.

Yao, J., Huang, C., and Li, D. (2015). Research on A Novel Ferrofluid Inertial Sensor with Levitating Nonmagnetic Rod. *IEEE Sensors J.* 16 (5), 1. doi:10.1109/JSEN.2015.2490253

Yu, M., Yang, C., Bian, X., Zhao, S., Wang, T., Liu, S., et al. (2016). Application of Fe78Si9B13 Amorphous Particles in Magnetorheological Fluids. *RSC Adv.* 6, 22511–22518. doi:10.1039/C5RA24106E

Yu, J., He, X., Li, D., and Li, W. (2018). Effective and Practical Methods to Calculate the Second-Order Buoyancy in Magnetic Fluid Acceleration Sensor. *IEEE Sensors J.* 18, 2278–2284. doi:10.1109/jsen.2018.2793944

Yu, J., Chen, D., Cai, Z., Li, D., Cao, Q., and Qian, L. (2019). Research on the Magnetic Fluid Levitation Force Received by a Permanent Magnet Suspended in Magnetic Fluid: Consideration a Surface Instability. *J. Magnetism Magnetic Mater.* 492, 165678. doi:10.1016/j.jmmm.2019.165678

Zubarev, A. Y., Odenbach, S., and Fleischer, J. (2002). Rheological Properties of Dense Ferrofluids. Effect of Chain-like Aggregates. *J. Magnetism Magnetic Mater.* 252, 241–243. doi:10.1016/s0304-8853(02)00674-1

Conflict of Interest: The authors declare that the research was conducted in the absence of any commercial or financial relationships that could be construed as a potential conflict of interest.

Publisher's Note: All claims expressed in this article are solely those of the authors and do not necessarily represent those of their affiliated organizations, or those of the publisher, the editors, and the reviewers. Any product that may be evaluated in this article, or claim that may be made by its manufacturer, is not guaranteed or endorsed by the publisher.